Registration of phase profile of coherent radiation and realization of adaptive control over laser beam in the presence of singular points in the wave front

F.Yu. Kanev, V.P. Lukin, and N.A. Makenova

Institute of Atmospheric Optics,
Siberian Branch of the Russian Academy of Sciences, Tomsk

Received April 22, 2002

The paper considers compensation for turbulent distortions of laser beams by an adaptive system including a Hartmann sensor. The control is realized under the conditions of singular points present in the radiation phase profile. To analyze the effect of dislocations on the accuracy of wave front registration, two algorithms of localization of singular points have been developed. The first algorithm is based on analysis of the phase surface of radiation and can be used only in a numerical experiment. In the second algorithm, dislocations are determined as branching points of interference fringes. This algorithm can be implemented experimentally. The accuracy provided by the both algorithms has been compared and the statistics of dislocations on the path has been obtained. The efficiency of phase conjugation was analyzed taking into account the restrictions introduced by the sensor. It is shown that the control loses its stability in the presence of dislocations, and a method is proposed to increase the stability.

Introduction

To close the feedback loop in the phase conjugation system, it is necessary to measure the phase profile of the reference beam.[1] Based on these measurements and depending on the particular realization of the control algorithm (several modifications of phase conjugation are known[2]), control signals for the final control element are generated. Therefore, one of the main elements of an adaptive system is a phase recording device, usually, the Hartmann sensor.[3]

The main principles of the sensor's construction are well known and thoroughly described in the literature.[3–5] Nevertheless, studying the sensor's operation under different conditions and the effect of its parameters on the accuracy of wavefront reconstruction, as well as optimizing its settings remain quite urgent tasks.

Selection of optimal number of subapertures is of primary practical interest. This problem for the telescope adaptive system was solved in Ref. 6, where the dependence of the point spread function on the number of sensor elements was determined. Another problem is choosing the shape of the lenses forming the focusing element. Lenslets with round, square, and hexagonal subapertures, as well as those formed by polar segments were considered in Ref. 7. That paper presents data on recording of Zernike polynomials and the phase profile of a beam distorted during its propagation through the atmosphere. The least errors were noticed for the sensor with square lenses and elements in the form of polar wedges.

A possible way to extend the dynamic range was proposed in Ref. 8. It was suggested to use a scanning sensor with only one subaperture moving within the range, where the phase is measured. In this case, centroid displacements are recorded by the entire light-sensitive element, rather than by its part corresponding to some subaperture. A shortcoming of this method is its lower speed.

Recording under the conditions of development of dislocations, when the reference wave phase is broken, can be considered as an individual problem. It was analyzed in Ref. 9, but no radical solution was found, only the need in obtaining additional results was underlined.

The brief overview of the above literature shows that the Hartmann sensor operation in the adaptive system is not completely studied yet. Optimization of the sensor and its use in correction of beam distortions and in wavefront measurements in the presence of singular points are the fields of further investigations. Some of these problems are solved in this paper by numerical methods. In Section 2, we consider algorithms for registration of dislocations, compare their accuracies, and reveal the peculiarities in manifestation of singular points on the path of beam propagation through the turbulent atmosphere. In Section 4, the results obtained are used to study correction of distortions in a system including the sensor. It is shown, in particular, that the presence of singular points leads to the complete breakdown of adaptive control – correction efficiency at adaptation is lower than at the open feedback loop. A possible solution of the problem is considered in this paper as well.

1. Radiation propagation model and a scenario of numerical experiment

In the numerical model used, the beam propagation through the turbulent randomly inhomogeneous atmosphere is described by the parabolic equation[10]:

$$2ik\frac{\partial E}{\partial z} = \frac{\partial E}{\partial x^2} + \frac{\partial^2 E}{\partial y^2} + k^2\tilde{n}(x, y)E, \qquad (1)$$

0235-6880/02/11 926-08 $02.00

where E is the complex field amplitude; z is the longitudinal coordinate; x and y are the coordinates in the plane normal to the beam propagation direction; k is the wavenumber. When solving Eq. (1), the longitudinal coordinate was normalized to the diffraction length $Z_d = ka_0^2$, and the cross coordinates were normalized to the initial beam radius a_0; $\tilde{n}(x, y)$ is the random field of refractive index fluctuations characterized by the structure function $D_n(\rho)$ (Ref. 4) corresponding to the 2/3 law:

$$D_n(\rho) = C_n^2 \rho^{2/3}, \quad (2)$$

where C_n^2 is the structure constant; $\boldsymbol{\rho} = (x, y)$, $\rho = |\boldsymbol{\rho}|$ are the coordinates of a point. The spectrum of fluctuations $\Phi_n(\kappa)$ was described by the Karman model

$$\Phi_n(\kappa, l) = 0.033\, C_n^2(l)\, (\kappa_0^2 + \kappa_m^2)^{-11/6}\, e^{-\kappa^2/\kappa_m^2};$$
$$\kappa_0 = 2\pi/L_0,\ \kappa_m = 5.92/l_0, \quad (3)$$

l_0 and L_0 are, respectively, the inner and outer scales of turbulence. For the spectral density of the model specified as

$$F_S(\kappa) = 2\pi\kappa^2 \int_0^L dl \Phi_n(\kappa) =$$
$$= 2\pi\kappa^2 0.033(\kappa^2 + \kappa_0^2)^{-11/6} e^{-\kappa^2/\kappa_m^2} \int_0^L dl C_n^2(l)$$

(L is the turbulent layer thickness), the parameter (Fried radius) characterizing the turbulence intensity is introduced:

$$r_0 = \left[0.423k^2 \int_0^L C_n^2(l) dl \right]^{-3/5}.$$

Turbulence in the simulation was represented by a single random phase screen located on the radiation propagation path (position of the screen on the path varied), as well as by a set of several screens. Specifying distortions by one screen does not correspond to the actual conditions, but allows us to consider various situations that help in understanding of the dislocation origination and phase control peculiarities.

To characterize residual distortions and the compensation efficiency, we used the focusing criterion

$$J(t) = \frac{1}{P_0} \iint \rho(x, y) I(x, y, z_0, t) dx dy, \quad (4)$$

having the meaning of the relative part of radiation power falling within the aperture of a preset radius, where P_0 is the total beam power and $\rho(x, y) = \exp[-(x^2 + y^2)/a_0^2]$ is the aperture function.

Beam control was realized based on the phase conjugation algorithm,[1] according to which the beam phase in the transmission plane was specified as

$$\varphi(x, y) = -\psi(x, y), \quad (5)$$

where $\psi(x, y)$ is the phase of the reference radiation.

2. Algorithms for registration of singular points. Origination and statistics of dislocations

A characteristic peculiarity arising at laser radiation propagation through the turbulent atmosphere is the appearance of singular points in its phase.[11] Some authors call these points dislocations,[12] while others call them optical vortices.[13] By optical vortex is meant a contour on the phase surface, the integral over which is equal to 2π.

In this section, we modify the well-known algorithms for detection of singular points, estimate the accuracy of their operation, determine the statistics of dislocations at different distances from a thin distorting screen and in the layer of turbulent medium, and note some characteristic peculiarities arising at appearance of dislocations. The conclusions drawn in this section are used by us in adaptive beam control.

To develop the algorithms and estimate their accuracy, we have constructed the model of an artificial optical vortex. The model is a surface with a 2π break beginning at the edge and ending at the center. If this surface is assigned to a Gaussian beam as a phase, then its interference pattern has branching fringes, that is, one of the methods to find singularities is the detection of branching points. Another known method[14] is the registration of local minimum points in the beam amplitude and calculation of phase incursion over a contour drawn around the minimum point. For a dislocation point, the incursion should be equal to 2π. Likely, the use of this algorithm not always gives correct results. For beam distortions to change the amplitude profile, the beam should pass a finite distance, whose length depends on the phase. Therefore, if the distance between the plane, whose phase was distorted by an optical vortex, and the registration plane is not large enough, then the change in the beam amplitude may fail to manifest itself.

We used two algorithms for localization of dislocations. The *first algorithm* analyzes the phase surface of the beam, while the amplitude distribution is not included in the analysis. The whole surface is divided into squares with variable size. The phase incursion along the square perimeter is determined. If the incursion is roughly equal to 2π, then the square is believed containing a singular point. The surface is checked for singularity only in the given region, beyond which dislocations are not determined. Technically, this is realized very simply – the phase beyond the region is set equal to zero. Application of the algorithm to the phase profile shown in Fig. 1*a* is illustrated in Fig. 1*b*, where the regions with zero phase (dark surface) are seen.

The whole surface is divided into squares. Four squares with singular points are marked in Fig. 1.

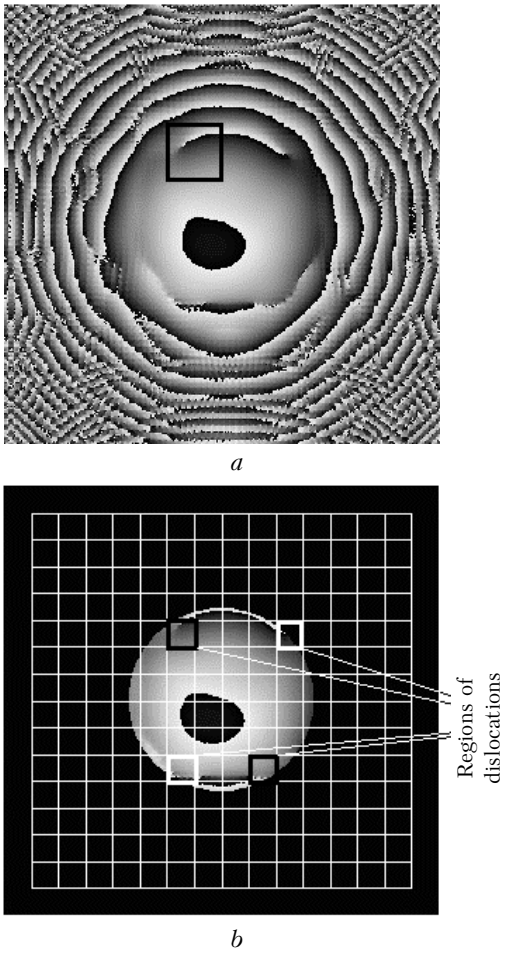

Fig. 1. Phase profile of the beam having singular points (*a*) and illustration of operation of the algorithm for determination of dislocations based on analysis of the phase surface (*b*).

One of the interesting problems, which can be solved using this model, is studying the dislocation origination process and determining the statistics of singular points at the propagation path. Here we present a brief study, since the main goal of this work is the compensation for turbulent distortions, rather than complete solution of the so-called phase problem. The statistics of dislocations in the beam having passed through a thin turbulent layer and then propagating in the vacuum is shown in Fig. 2. Registration was performed in the area with the radius equal to the beam energy radius σ:

$$\sigma(t)=\left[\frac{1}{P_0 a_0^2}\iint(\mathbf{r}_\perp-\mathbf{r}_c)^2 I(x,y,z_0,t)\,\mathrm{d}x\mathrm{d}y\right]^{1/2},$$

where $\mathbf{r}_\perp = \{x, y\}$ is the coordinate vector of a point on the plane; $\mathbf{r}_c$ is the coordinate vector of the beam energy centroid.

As is seen from Fig. 2, there are almost no dislocations ($z \le 0.05$, $r_0 = 0.1$) or a few (at $r_0 = 0.05$ and 0.03) at a small distance z behind the screen.

Then phase distortions are transformed into amplitude ones, but the beam phase also changes – the number of singular points increases drastically (interval $z = 0.05$, 0.3). Then their number changes only slightly and a saturation of N_{dsl} is observed at $z > 0.3$.

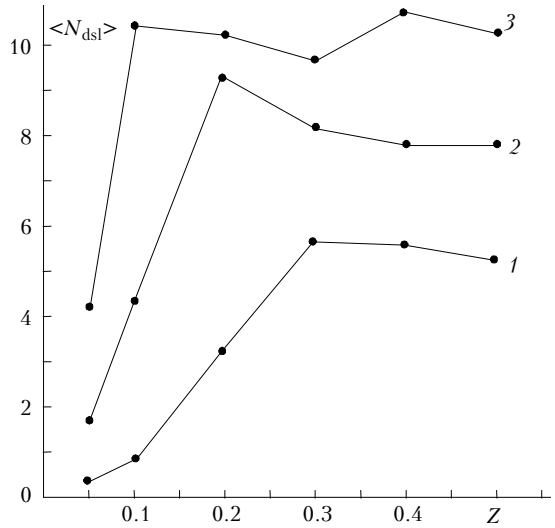

Fig. 2. Statistics of dislocations on the beam propagation path. The data are obtained from averaging over 50 realizations. Turbulence is simulated by one screen located at the beginning of the path. Singular points are localized using the algorithm of phase surface analysis; $r_0 = 0.1$ (curve *1*), 0.05 (*2*), and 0.03 (*3*).

The process of the dislocation origination is illustrated in more detail in Fig. 3. This figure shows the phase profile of the beam at different distances from the distorting screen (the screen is placed immediately ahead of the source aperture, $Z_s = 0$). If the distance z passed by the beam after introduction of distortions is small, the beam's phase in the central part is smooth and singularities are absent. Surface irregularity in the central area and at the periphery is explained by computational peculiarities.

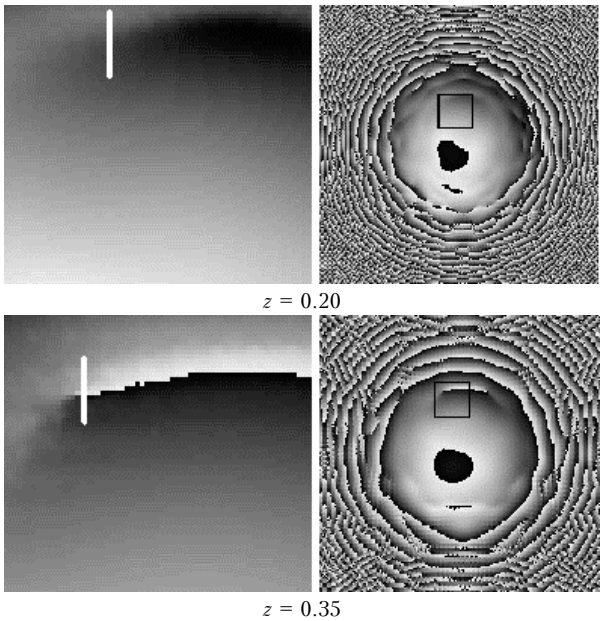

Fig. 3. Origination of dislocations on the beam path. The white line on the left is a part of the contour, over which phase incursion is summed up.

The profile $\varphi(x, y)$ in the problem can be found as

$$\varphi(x, y) = \mathrm{Arg}\,[\mathrm{Im}(E)/\mathrm{Re}(E)], \qquad (6)$$

where $\mathrm{Im}(E)$ is the imaginary part and $\mathrm{Re}(E)$ is the real part of the complex amplitude of the field E. The function Arg( ) is determined in the range $0-2\pi$. If $\varphi(x,y)$ is beyond this range, the result of computation is a surface break. Additional distortions are introduced by the noise characteristic of the considered conditions.

At the distance $z = 0.2$, a fold arises in the phase surface, and then this fold is transformed into an optical vortex. In the expanded scale, the vicinity of an incipient dislocation is shown in the left part of Fig. 3 together with a portion of the contour (white line), along which the phase surface is rounded. The corresponding values of the phase are given in Fig. 4*a*, which demonstrate that it is not a dislocation, because a break is absent. As the distance, passed by the beam, increases ($z = 0.35$), a break arises in the considered region. This is seen in Fig. 3 (dislocation is especially well seen in the expanded scale) and in Fig. 4, which gives the phase values for the marked part of the contour. The break for two neighboring points is almost 2π.

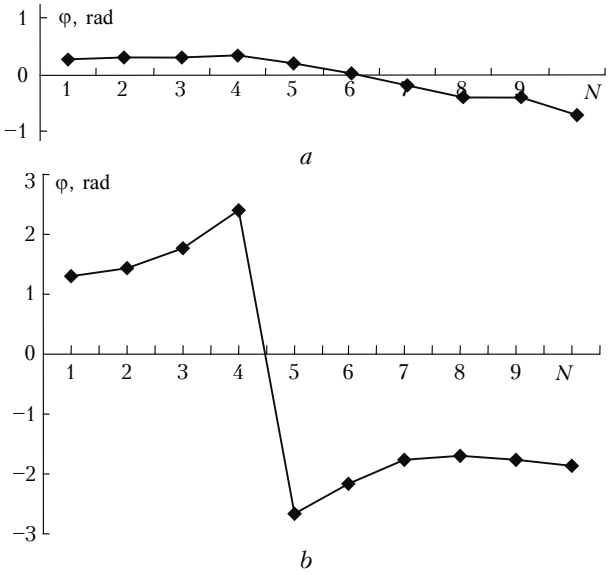

Fig. 4. Phase variation at the marked fragment of the contour at $z = 0.20$ (*a*) and 0.35 (*b*); N is the number of the contour point.

Thus, for development of dislocations in the turbulent medium, a beam should pass some finite distance after the distorting layer. Likely, all singular points arise almost simultaneously, and this can explain the drastic increase of their number in a short range of the distance. Then the number N_{dsl} keeps almost unchanged – all dislocations already have arisen and remain within the registration plane. It should be also noted that the number of dislocations increases as the turbulence intensity increases. In Fig. 2, the curves obtained at smaller r_0 are located above the curves corresponding to the larger r_0.

Another characteristic peculiarity of distribution of dislocations in the beam is illustrated in Fig. 5. Here the average number of singular points in different beam sections is presented, that is, the dependence of N_{dsl} on relative sizes (diameter D_{dsl}) of the zone, in which a dislocation is determined. The beam passes through a thin turbulent layer located at the very beginning of the path, and is recorded in the plane located at $z = 0.5$ from the source aperture. It can be seen that, regardless of the intensity of turbulent distortions, dislocations are almost absent in the central part of the beam ($N_{\mathrm{dsl}} \approx 0$ in the zone with the relative diameter of 0.4 of the beam energy diameter). As the diameter increases, N_{dsl} grows by almost the square law. It should be noted here that noise at the beam edges (or errors of the grid representation of the functions) increases significantly, while the accuracy in determination of dislocations decreases sharply. Therefore, it is impossible to reliably determine what causes the increase in N_{dsl}: errors or other factors.

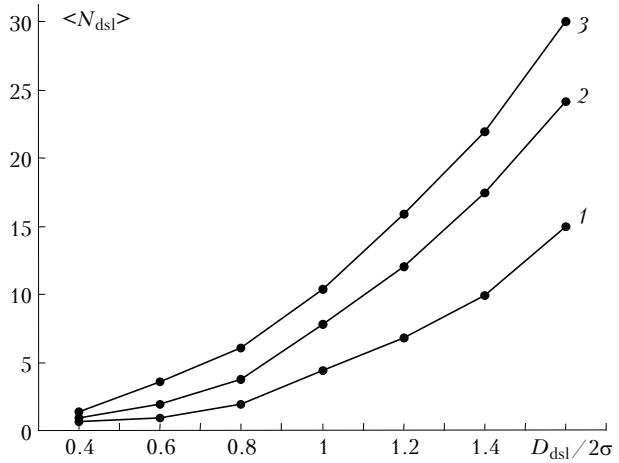

Fig. 5. Dependence of the number of dislocations $\langle N_{\mathrm{dsl}}\rangle$ on the relative size of the zone (D_{dsl} is the zone diameter, σ is the beam energy radius). Results are averaged over 50 realizations. Parameters of the problem: $z = 0.5$, the turbulent screen is located at the beginning of the path; $r_0 = 0.1$ (curve *1*), 0.05 (*2*), and 0.03 (*3*).

In general, it can be concluded that the above algorithm allows determining singular points in the phase profile of the Gaussian beam with sufficient reliability. At the same time, it has a significant shortcoming – it cannot be realized experimentally.

Therefore, the *second algorithm* used by us in this work is based on analysis of the interference pattern. It determines dislocations as branching points of interference fringes. To increase the accuracy of the method, we propose its following modification. The whole phase surface is divided into squares. The phase within each of the squares is assigned to the Gaussian beam, for which the interference pattern is recorded. This pattern is then subjected to the operation of skeletonization – the fringe intensity at a certain level is set equal to unity, and the intensity below this level is zero (the scheme is shown in Fig. 6).

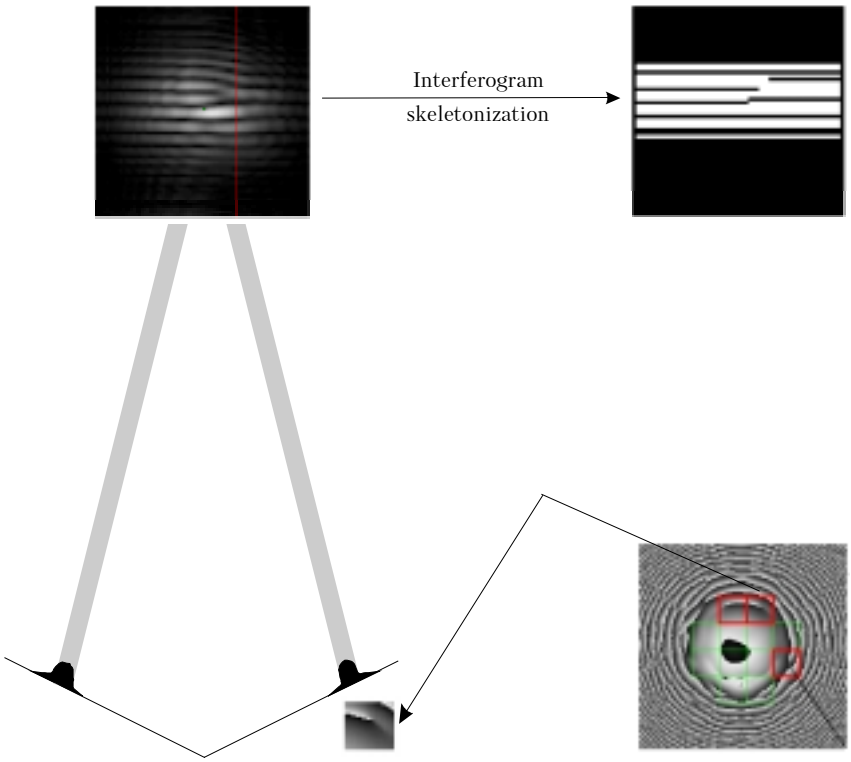

Fig. 6. Algorithm for localization of dislocations based on analysis of interference pattern.

Branching points are sought in the obtained skeleton of interferogram. If such a point is detected, it is assumed that a dislocation is present in the corresponding square, otherwise a dislocation is thought absent in that square. The algorithm allows determining singular points in subapertures of the Hartmann sensor – interference is analyzed for each of the beams having passed a subaperture.

On the path of the beam having passed through a thin turbulent layer, the number of dislocations determined by the second algorithm roughly coincides with the results given by the first algorithm.

All above data were obtained when simulating distortions by one phase screen, that is, under the condition that the beam passes through a thin turbulent zone. Of practical interest is to study radiation propagation in the turbulent atmosphere, when the distorting volume has a finite, nonzero length. Peculiarities of dislocation appearance under such conditions are illustrated by Fig. 7 (similar to Fig. 2), which gives the number of singular points in different planes of the propagation path. The difference is that now the registration planes are within the distorting layer. But the features of dislocation development are the same – dislocations are absent at the beginning of the path (at a small distance from the first phase screens) and then they arise almost simultaneously (sharp growth of the curves). Here we can hardly speak about saturation of the number of singular points – new distorting layers must introduce additional optical vortices, therefore the behavior of the plots after the drastic increase is rather complex.

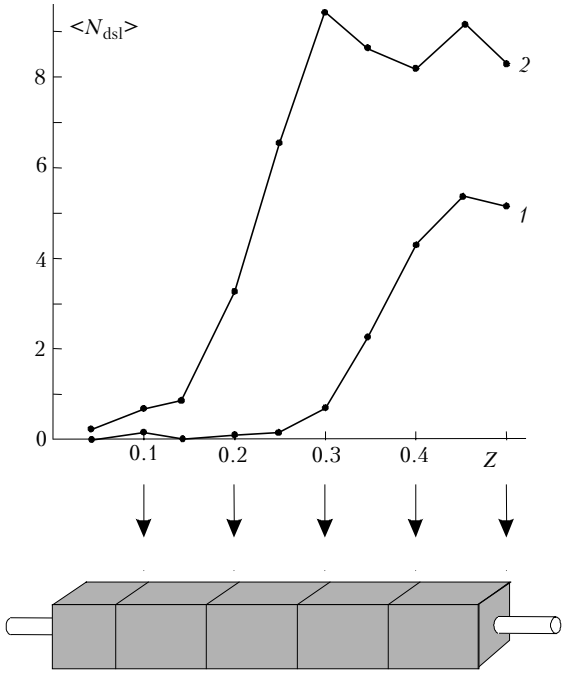

Fig. 7. Statistics of dislocations in different planes of the turbulent layer. The data are averaged over 50 realizations: r_0 = 0.02 (curve *1*) and 0.01 (*2*).

The distribution of the number of dislocations in the beam cross section is the same as in the case of one screen – the phase surface in the central zone is smooth with no singular points.

3. Model of the Hartmann sensor

In real adaptive-optics systems, beam phase is registered by the Hartmann sensor[3] consisting of a set of lenses (lenslets) in a case or of a transparent plate formed by several lenses. A lenslet focuses the incident radiation. A high-resolution video camera or a photodetector array divided into plates, each corresponding to one subaperture (lens), is usually installed in the sensor's registration plane. The beam energy centroid shift is measured within the plate and then used for calculation of the local (within the subaperture) wavefront tilt. The phase surface of radiation coming to the sensor is reconstructed from the local tilts by the least-square method.

The sensor model was constructed by the simplified scheme (Fig. 8). The wave front of the beam having passed through the turbulent atmospheric layer was used as an input information, and the result was the surface reconstructed from local tilts.

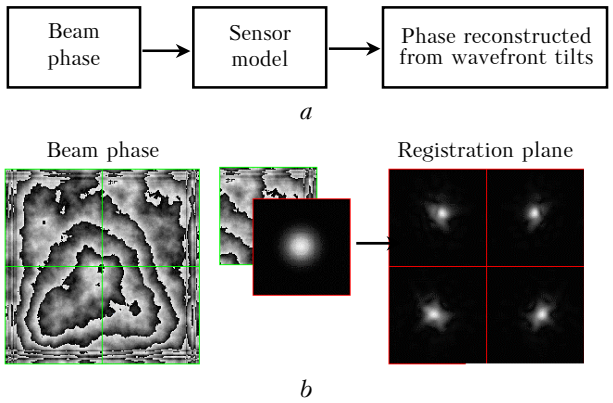

Fig. 8. Simplified model of the Hartmann sensor: functions executed by the model (*a*), realization of the algorithm (*b*).

In the algorithm developed, the wave front was divided into squares, a part of the phase surface falling within a square was assigned to the Gaussian beam, and then the problem of radiation propagation in vacuum was solved. The centroid shift was determined in the registration plane and then used for calculation of the local tilt. This operation was performed for each subaperture. The total surface was reconstructed by the least-square method. This scheme does not correspond exactly to the real sensor described above, but its application nevertheless seems worthwhile, since, unlike the complete model, this one is easy to adjust and use, and the results obtained can be readily interpreted.

The program provides for the following capabilities:

1. To vary the number of subapertures from 4 (2×2) to 256 (16×16), the distance from a lenslet to the observation plane, and the lenslet focal length (the focal length is the same for all lenses).

2. To change the *beam/subaperture radius* ratio (subaperture filling by the beam).

3. To represent visually the algorithm operation, to display phase surfaces and amplitude distributions.

4. To specify the phase surface by the lowest Zernike polynomials and to determine the errors of polynomial reconstruction.

5. This program can be used as a component of a distributed application. In this case, the phase surface is transmitted from the program simulating radiation propagation and then the reconstructed surface is returned.

4. Adaptive control in the presence of dislocations

At adaptive beam control, the main characteristic of the accuracy of the sensor operation is the efficiency of correction for distortions. We characterize the quality of compensation by the criterion J proposed in Section 1, which is proportional to the radiation power falling within the subaperture of a preset size. In the numerical experiments, we used a simplified model of the sensor and simulated the turbulence by one screen (a thin turbulent layer) located immediately forward of the source aperture or at a finite distance from the aperture. In the first case, the beam parameters were registered immediately behind the screen and, as was shown above, dislocations were absent in such measurements. As the turbulence intensity increased, the phase surface registered by the sensor became more complex, but singular points did not show themselves. The results of the control obtained at different fillings of the subaperture are shown in Fig. 9. If $D_{sub}/D_b \gg 1$, then the sensor aperture is absolutely transparent, and as this ratio decreases, the diameter of the transparent zone decreases as well.

To compare the operation of an ideal device of phase registering (curve *1* in Fig. 9 is obtained using an ideal sensor providing the maximum value of the criterion) and the model of a sensor with 64 (8 × 8) subapertures, Fig. 9 presents the values of J obtained as a result of control with these two devices. This figure also gives the data on the direct beam propagation (curve *4*, the open feedback loop, no correction).

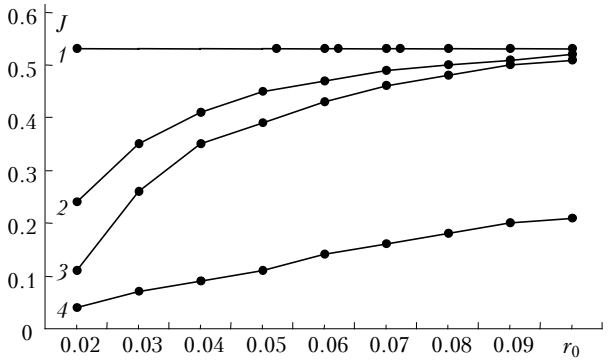

Fig. 9. Dependence of the efficiency of adaptive correction on the intensity of turbulent distortions at different fillings of subaperture by the beam (the number of subapertures is 8 × 8, the screen is located at the zero distance from the transmitting aperture): ideal sensor (curve *1*), the aperture/beam radii ratio is 2.0 (*2*) and 7.5 (*3*), no control (*4*).

It can be seen from Fig. 9 that for any values of the Fried radius the ideal sensor provides the complete compensation of turbulence. The efficiency of the system including the real sensor decreases with the increase in the intensity of distortions (at decreasing r_0). This happens because the accuracy of registration of a complex curve is lower than that of a simple curve (curve *2*). As the diameter of the transparent zone in the subaperture decreases, the accuracy decreases more quickly with the decrease of r_0 (curve *3*).

It was underlined in Section 1, that simulation of turbulence by one screen allows a more detailed analysis of the problem under consideration as compared to the experiment, where the atmosphere is represented by a distributed randomly inhomogeneous lens. In particular, we can recognize two cases: sensor operation in the absence of dislocations in the reference beam (as described above, turbulence is simulated by a screen located at the beginning of the path) and phase registration in the presence of dislocations. Singular points arise only when the beam has passed some finite distance after the distorting screen. This condition is fulfilled if the screen is placed at the path's center or at some other nonzero distance Z_s from the source aperture. For such a scenario, the reference beam phase radically differs from the phase obtained at zero distance from the screen – dislocations arise in it.

Control under these conditions has the following peculiarities. First, complete compensation of distortions is impossible even with an ideal sensor. Therefore, the criterion J decreases with decreasing r_0 even in the ideal system (curve *1* in Fig. 10).

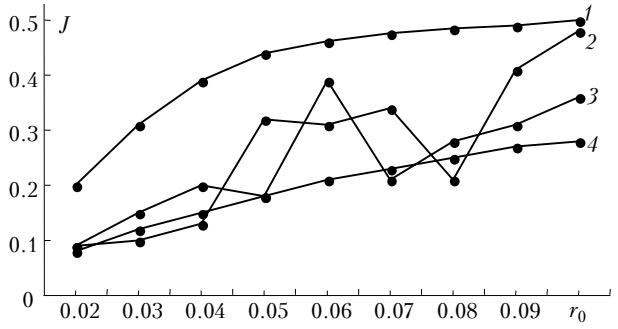

Fig. 10. Data similar to that shown in Fig. 9. The distorting screen is located at the distance of 0.25 from the source aperture (at the path center).

The decrease in the efficiency is explained by violation of the principle of optical reversibility at correction. For the condition of complete compensation to fulfill, at the entrance to the medium we should form a beam with the imaginary part of the complex field amplitude opposite in sign to the imaginary part of the reference beam:

$$\mathrm{Im}(E_{\mathrm{beam}}) = -\,\mathrm{Im}(E_{\mathrm{beacon}}), \qquad (7)$$

where $\mathrm{Im}(E_{\mathrm{beam}})$ is the imaginary part of the amplitude of the direct beam, and $\mathrm{Im}(E_{\mathrm{beacon}})$ is that of the reference beam. Physically, this operation means that a beam with the amplitude profile coinciding with the reference beam profile and the phase opposite to the phase of the reference beam is specified at the entrance into the medium, that is, wave front reversal (WFR) is performed. The use of WFR results in complete compensation of the turbulent layer located at any distance from the laser source. If the amplitude is specified with deflection from the required one, then the efficiency of correction decreases, as exemplified by the data shown in Fig. 10. Further decrease of the efficiency is observed with the Hartmann sensor included into the system. Phase conjugation in such a system is unstable (curves *2* and *3* in Fig. 10). This is explained by two types of errors made at correction: violation of the principle of optical reversibility (replacement of WFR by phase conjugation) and the presence of dislocations in the reference beam.

All above results were obtained for one of realizations of a random phase screen, that is, for the statistical problem of adaptive control of the beam in the turbulent atmosphere. The conclusions drawn should be confirmed by the data obtained from averaging. The computations needed were performed for the scenario that the screen was located at the path center, and the results of these computations are shown in Fig. 11. As in the previous experiments, with increase of the turbulence intensity, compensation for the screen located at the finite distance from the source aperture becomes inefficient because of dislocations, and the obtained values of the focusing criterion are even lower than at the open feedback loop. In the absence of dislocations, the sensor operates with a satisfactory accuracy, which decreases with the decrease of r_0, that is, the main regularities of the control are the same as in the case of compensation for one of the screen realizations.

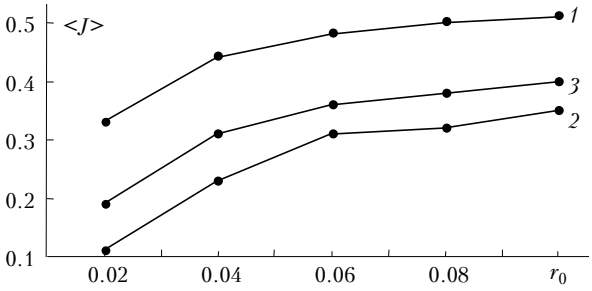

Fig. 11. Efficiency of adaptive correction with the use of the Hartmann sensor. Averaging is performed over 50 realizations. The screen is located at the path center. The system includes the ideal sensor (*1*), the Hartmann sensor with 8×8 subapertures (*2*), and no control (*3*).

All above results were obtained for the sensor with the diameter seven times larger than the beam diameter, and optimization of the size parameters was not performed. At the same time, it follows from the data of Fig. 5 that dislocations are concentrated in the periphery zone, that is, when decreasing the sensor size, it is possible to decrease the number of singular points in subapertures or to completely exclude them. Therefore, numerical experiments aimed at optimization of the receiver's diameter were conducted. The results of control

with the sensor, whose diameter is 1.5 of the beam energy diameter, are depicted in Fig. 12 (the screen was located at the path center, and dislocations were present in the reference beam). It is seen from Fig. 12 that in some realizations the focusing criterion decreases monotonically with the increase in the intensity of distortions. This means that the control stabilization was obtained (curve *2*). The averaged values of the criterion (curve *1*) are higher as compared to the experiment with the open feedback loop (the data for the case free of correction are presented in Fig. 10 for one realization, and Fig. 11 gives the averaged values of the criterion).

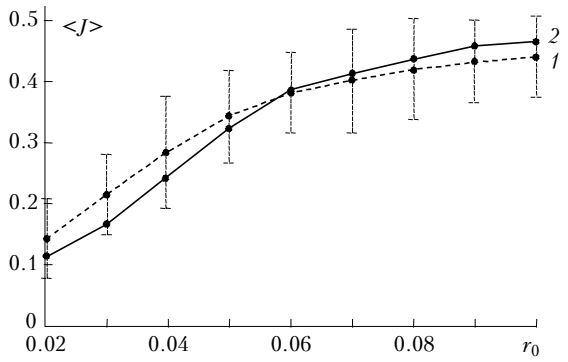

Fig. 12. The result of control with the Hartmann sensor having the optimal size (the screen at the path center) included in the system: averaging over 50 realizations (curve *1*) and one realization (curve *2*).

Thus, we have implicitly confirmed the conclusion that just dislocations lead to the control breakdown and illustrated the possibility to decrease the effect of singular points on the compensation for turbulent distortions.

References

1. M.A. Vorontsov and V.I. Shmal'gauzen, *Principles of Adaptive Optics* (Nauka, Moscow, 1985), 335 pp.
2. F.Yu. Kanev and V.P. Lukin, Atm. Opt. **4**, No. 12, 856–863 (1991).
3. Luis Diaz Santana Haro, *Wavefront Sensing in the Human Eye with a Shack–Hartmann Sensor* (Publishing House of London University, London, 2000), 97 pp.
4. V.P. Lukin and B.V. Fortes, *Adaptive Beaming and Imaging in the Atmosphere* (SB RAS Publishing House, Novosibirsk, 1999), 211 pp.
5. V.P. Lukin, F.Yu. Kanev, P.A. Konyaev, and B.V. Fortes, Atmos. Oceanic Opt. **8**, No. 3, 215–219 (1995).
6. V.P. Lukin, N.N. Maier, and B.V. Fortes, Atmos. Oceanic Opt. **5**, No. 12, 801–807 (1992).
7. V. Voitsekhovich, L. Sanchez, V. Orlov, and S. Cuevas, Appl. Opt. **40**, No. 9, 1299–1304 (2001).
8. V. Laude, S. Olivier, C. Dirson, and J.-P. Huignard, Opt. Lett. **24**, No. 24, 1796–1798 (1999).
9. P.R. Barbier, D.W. Bush, P. Polak-Dingles, and M.L. Plett, in: *Proc. of the 2nd International Workshop on Adaptive Optics in Industry and Medicine* (Durham, UK, 1999), pp. 352–357.
10. V.A. Vysloukh, V.P. Kandidov, S.S. Chesnokov, and S.A. Shlenov, Izv. Vyssh. Uchebn. Zaved., Ser. Fiz., No. 11, 30–41 (1985).
11. A. Primmerman, R. Pries, R.A. Humphreys, B.G. Zollars, H.T. Barclay, and J. Herrmann, Appl. Opt. **34**, No. 12, 2081–2088 (1995).
12. N.B. Baranova, A.V. Mamaev, N.F. Pilipetskiy, V.V. Shkunov, and B.Ya. Zel'dovich, J. Opt. Soc. Am. **73**, No. 5, 525–528 (1985).
13. V.P. Aksenov, V.V. Kolosov, V.A. Tartakovskii, and B.V. Fortes, Atmos. Oceanic Opt. **12**, No. 10, 912–918 (1999).
14. F.Yu. Kanev, V.P. Lukin, and L.N. Lavrinova, Atmos. Oceanic Opt. **14**, No. 12, 1075–1080 (2001).